Interface defect formation for atomic layer deposition of SnO2 on metal halide perovskites

Nitin Mallik, Javid Hajhemati, Mathieu Frégnaux, Damien Coutancier, Ashish Toby, Shan-Ting Zhang, Claudia Hartmann, Elif Hüsam, Ahmed Saleh, Thomas Vincent, et al.

Interface Defect Formation for Atomic Layer Deposition of SnO_2 on Metal Halide Perovskites

Nitin Mallik[‖], Javid Hajhemati[‖], Mathieu Frégnaux, Damien Coutancier, Ashish Toby, Shan-Ting Zhang, Claudia Hartmann, Elif Hüsam, Ahmed Saleh, Thomas Vincent, Olivier Fournier, Regan G. Wilks, Damien Aureau, Roberto Félix, Nathanaelle Schneider, Marcus Bär, Philip Schulz[*]

[‖]Contributed equally [*]Corresponding author

ABSTRACT: With the rapidly advancing perovskite solar cell (PSC) technology, dedicated interface engineering is critical for improving device stability. Atomic layer deposition (ALD) grown metal oxide films have drawn immense attention for the fabrication of stable PSC. Despite the advantages of ALD, the deposition of metal oxides directly on bare perovskite has so far not been achieved without damaging the perovskite layer underneath. In addition, the changes to the physicochemical and electronic properties at the perovskite interface upon exposure to the ALD precursors can alter the material and hence device functionality. Herein, we report on a synchrotron-based hard X-ray photoelectron spectroscopy (HAXPES) investigation of the buried interface between metal halide perovskite (MHP) absorber and ALD-SnO_2 electron transport layer. We found clear evidence for the formation of new chemical species (nitrogen compound, lead dihalides), upward band bending in the MHP, and downward band bending in the SnO_2 towards the MHP/ALD-SnO_2 interface. The upward bending at the interface forms an electron barrier layer of ~400 meV, which is detrimental to the PSC performance. In addition, we assess the effectiveness of introducing a thin interlayer of the organic electron transport material Phenyl-C61-butyric acid methyl ester (PCBM) between MHP and ALD-SnO_2 to mitigate the effects of ALD deposition.

Keywords: Metal Halide Perovskite, Atomic Layer Deposition, Metal Oxide, ALD-SnO_2, Buried Interface, Hard X-ray Photoelectron Spectroscopy.

1. Introduction

In recent years, metal halide perovskite (MHP) solar cells have attracted immense attention among researchers due to the rapid advances in power conversion efficiency (PCE) beyond 25%, which is now comparable to Si-based technologies.[1,2] Such extraordinary improvement of PCE in perovskite solar cells (PSCs) was made in light of the growing fundamental understanding of MHPs and improved interface engineering.[3,4] However, to this date, the long-term stability of PSCs, which is inherently affected by their interfaces, remains a key issue for widespread applications.[5]

The intricacy of the involved interfaces owes to the perovskite material itself, which often includes five to six different elemental and molecular components, among them readily reduced metal cations, acidic organoammonium cations, and reactive halide species.[6] The charge transport layers (CTLs) that form a direct interface with the MHP are also critical to the stability of PSCs.[7] Comparing different CTLs, inorganic materials (e.g., metal oxides) have demonstrated better stability than organic materials in response to heat, light, and the local chemical environment.[8] Recent studies demonstrated that the stability of PSCs can be improved through deliberately tailoring interface properties and by introducing a compact metal oxide layer on the MHP. Several of these studies report on the incorporation of metal oxide CTLs (TiO_2, SnO_2, and NiO) in PSCs reaching PCE above 20%.[9-12]

The problems, in general, occur when the CTL is deposited directly on a bare MHP film, as this can potentially damage the absorber layer. Therefore, it is essential to choose a suitable deposition process to limit such damage. In a few demonstrations, oxide layers such as aluminum or titanium oxides were implemented directly on top of perovskite layers using spin coating, sputtering, thermal evaporation, and atomic layer deposition (ALD).[13, 14] Not all techniques are suited equally well; sputter deposition for instance usually damages the perovskite layer due to high energy ion bombardment.[15] Furthermore, the thermal instability of

the perovskite materials limits the post-annealing temperature for the oxide growth when using spin coating and thermal evaporation.[16]

In contrast, ALD is promising for growing oxide layers directly on top of MHP films due to its relatively low deposition temperature, uniform coverage, and industrial scalability.[17,18] However, even this comparably "soft" deposition process can damage the MHP underneath due to the reliance of ALD on chemical precursors and reactions.[19,20] The reported PSCs, with ALD oxide deposited on top, have generally shown low PCEs in the range of 0.5%-8.2%.[21-28]

In a recent fundamental interface study of $Cs_{0.05}FA_{0.79}MA_{0.16}PbBr_{0.51}I_{2.49}$ MHP and ALD SnO_x, where FA and MA stand for formamidinium and methylammonium respectively, Hultqvist et al. observe the formation of additional chemical species involving Pb, Br, and N at the interface and suggest that this causes the formation of a barrier layer.[29] Aside from these select examples, there is a significant lack of fundamental research and hence understanding of the chemical interaction of the MHP surface with ALD precursors during the metal oxide preparation. In particular, its impact on the energy level alignment and hence electronic properties remains a key target for further investigation. These insights are, however, essential prerequisites for developing damage-free ALD metal oxide deposition processes for MHPs. Thus, they serve as the basis and motivation of this work.

In our study, we present a synchrotron-based hard X-ray photoelectron spectroscopy (HAXPES) interface study of $FA_{0.7}Cs_{0.3}Pb(I_{0.9}Br_{0.1})_3$ MHP with thin ALD SnO_2 overlayers (see Figure 1) using two different photon energies (2 and 6 keV) for excitation that provide different information depths and hence assess the surface and interface properties, respectively. This study utilizes a double cation mixed halide perovskite devoid of MA owing to its superior thermal and moisture stability, rendering it better suited to withstand the ALD process.[30] Our investigation yields evidence of chemical defects at the MHP/metal oxide interface due to reaction between MHP and ALD precursors with these chemical defects causing an upward band bending in the MHP that results in a barrier for electron extraction at the MHP/SnO_2

interface. In an attempt to mitigate this, we also studied samples with Phenyl-C61-butyric acid methyl ester (PCBM) as an organic buffer layer between MHP and ALD SnO_2.

2. Results and discussion

The device architectures used in this interface study are comprised of F-doped tin oxide(FTO)-coated glass substrate, NiO, $FA_{0.7}Cs_{0.3}Pb(I_{0.9}Br_{0.1})_3$ MHP with and without a 40 nm PCBM buffer layer, and ALD SnO_2 (see Figure 1(b)). For this HAXPES-based interface study, 30 cycles of ALD SnO_2 are deposited on top of glass/FTO/NiO/MHP(/PCBM) samples (see Figure 1(a) for a schematic presentation of the ALD cycles, see supporting information for more details). This corresponds to a 5 nm thick ALD SnO_2 film grown on a reference Si substrate in the same deposition run. However, note that the growth rates can differ for various substrates (see supporting information, S.I., Section 1.2).

Figure 1(c) illustrates the X-ray diffraction (XRD) patterns of the bare MHP film, with ALD-SnO_2, PCBM, and PCBM/ALD-SnO_2 overlayers. Comparing the XRD patterns of all samples, we observe a low-intensity PbI_2 peak at 12.5° for the samples with the ALD-SnO_2 layer on top. As this MHP is found to be thermally stable at 100 °C (see S.I., Figure S1), we attribute the formation of the PbI_2 peak to the chemical reaction between the MHP layer and the ALD precursors. Even the use of a protective PCBM interlayer does not fully inhibit this reaction (as indicated by the smaller but visible PbI_2 related peak in the corresponding X-ray diffraction data). The presence of PbI_2 is also observable in the absorbance spectra of the samples with ALD-SnO_2 as shown in Figure 1(d) as a slight increase starting at a wavelength of around 515 nm (i.e., the band gap of PbI_2) and rising toward the UV-region.[31] We see that while the samples with ALD-SnO_2 present higher absorption in the wavelength range between 400 nm and 550 nm, the absorption becomes slightly lower for wavelengths longer than 550 nm. The samples containing a PCBM interlayer demonstrate increased absorption in the wavelength range between 400 to 650 nm, as indicated by the orange/red spectra, in contrast to the sample

without a PCBM interlayer, represented by the green/blue spectra. We attribute this observation to the parasitic absorption in the PCBM film itself. The long-wavelength absorption onset at 750 nm is attributed to the fundamental absorption onset of the used double cation MHP.

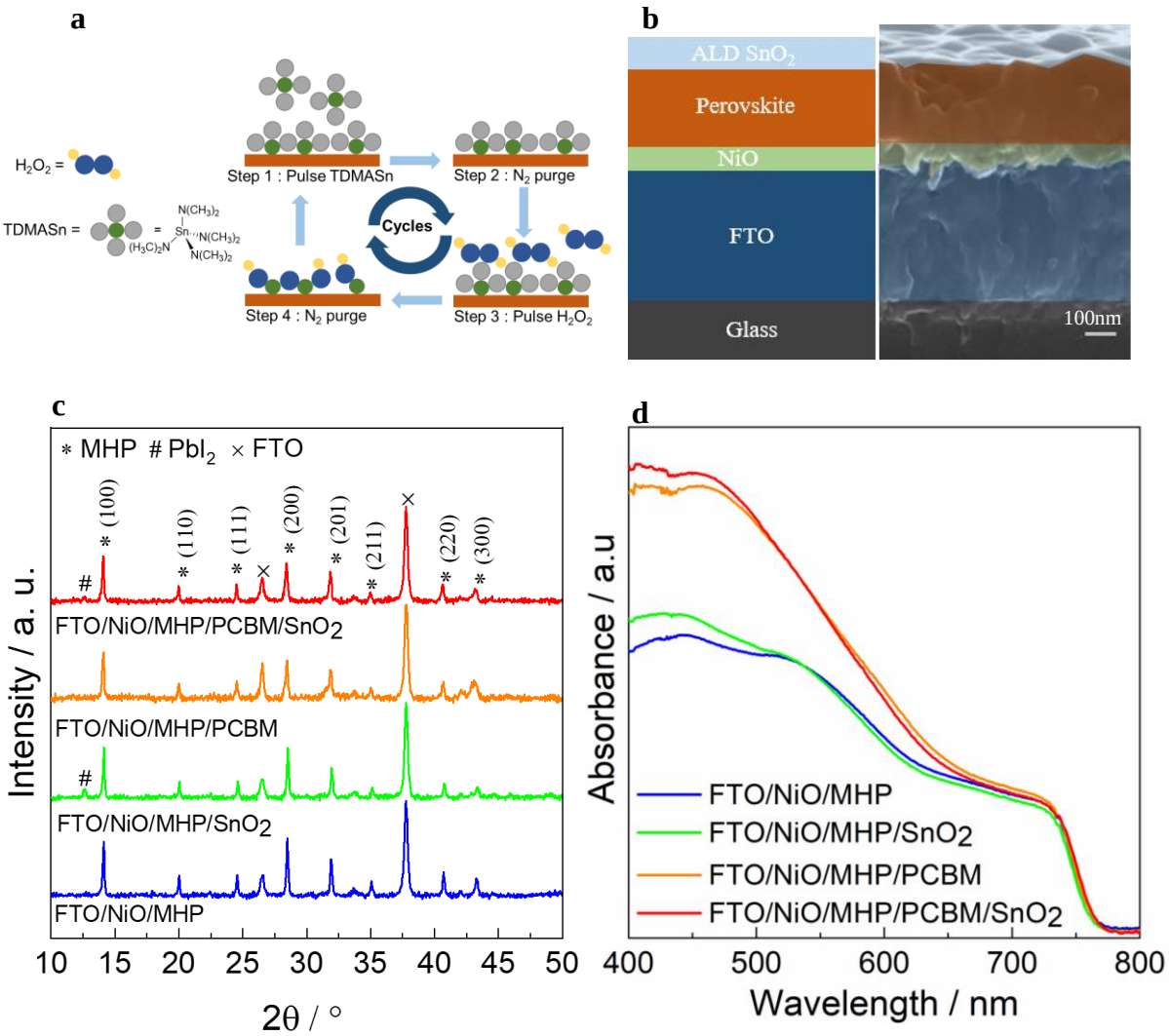

Figure 1. (a) Simplified schematic of the ALD process with Tetrakis(dimethylamido)tin(IV) (TDMASn) and H_2O_2 precursors to form SnO_2 layers. (b) Schematic of the investigated half-device stack of a P-I-N MHP based solar cell configuration without PCBM and corresponding cross-sectional SEM image. (c) XRD pattern of double cation MHP films with and without (PCBM/) ALD-SnO_2 top layers. (d) UV-Vis absorption spectra of samples with and without (PCBM/) ALD-SnO_2 top layers.

The HAXPES spectra of the Cs $3d_{5/2}$, N 1s, Pb 4f, I 3d, Sn $3d_{5/2}$, and O 1s core level regions of the bare MHP samples and after ALD SnO_2 deposition are depicted in Figure 2. The intensities of the various MHP core levels are normalized to maximum intensity for better data visualization. The I 3d and Pb 4f core level signals of pristine MHP show a minor shift in peak position (10-100 meV) between the data acquired for photon energies of 2 keV and 6 keV, respectively (see S.I.,Table S2). Considering the spectral resolution of our HAXPES experiment, we do not consider a shift of this order of magnitude to be significant.

The deposition of SnO_2 results in a larger shift of the lead and iodine core levels by approximately 200 and 300 meV to lower binding energies, respectively. These peak shifts are presumably indicating a change in electronic structure (i.e., band bending), which can be caused by defect formation at the interface; notably this coincides with the formation of PbI_2 that we observed by XRD. We also monitored and compared the ratio of iodine to lead at the surface and subsurface of the perovskite layer before and after the ALD-SnO_2 deposition (see S.I., Table S3). The quantification shows that before SnO_2 deposition, the I/Pb ratio near the MHP surface is 2.7 i.e., almost equal to the expected stoichiometry value, decreasing to 2.4 with increasing probing depth. After SnO_2 deposition, we observed a more severe iodine deficiency and a contrary I/Pb profile, i.e., the deficiency is more apparent in the 2 keV measurements, in which the calculated I/Pb ratio is 0.7, i.e., almost one fourth of the initial stoichiometric ratio. In comparison, we find the ratio to be higher (1.7) in the more bulk-sensitive 6 keV measurements, indicating that this I depletion is driven by the interface formation with the SnO_2 or its synthesis process. Halide deficiency forms deep-level defects in the metal halide perovskite solar cells, which likely increases interfacial charge recombination and impede carrier extraction, negatively affecting PSCs performance.[32]

Upon SnO_2 deposition, a new peak appears at 138.9 and 139.2 eV (for 2 and 6 keV photon energy, respectively) in the Pb 4f core-level spectra for the MHP/SnO_2 sample, which corresponds to the Sn 4s core level. The shift in binding energy of Sn 4s core level could be

related to band bending in the SnO_2 film; however, the precision of the fit is significantly affected by the adjacent Pb 4f core level fitting. Therefore, testing this hypothesis required further analysis of the Sn 3d and O 1s core levels, as presented below.

However, first we closely inspect the N 1s spectra, for which a new nitrogen peak is observed at 398.7 eV in case of the MHP sample with ALD-SnO_2. The relative intensity of this peak is higher at 2 keV excitation, indicating that the nitrogen species causing this N 1s contribution is predominantly present within the ALD-SnO_2 layer or at the MHP/ALD-SnO_2 interface. Note that the corresponding peak intensity using 6 keV photon energy is close to the detection limit. The formation of a new chemical state of the nitrogen species (N^*) at the MHP interface would be consistent with an interfacial chemical reaction, as has been suggested before.[27]

The emergence of the detected nitrogen species can be attributed to two potential origins: firstly, as a reaction/degradation product of the ALD precursor such as dimethylamine derivative, and secondly, as a degradation product arising from the formamidinium (FA) species present within the MHP structure. A plausible candidate for this degradation product is the *sym*-triazine, a nitrogen-containing heterocycle recognized as 1,2,5-triazine.[33,34] We note that the presence of *sym*-triazine at a FA-based halide perovskite/ALD-SnO_2 interfaces was further corroborated by FTIR measurements in a recent study.[35]

Furthermore, the N 1s peak around 400 eV related to the FA species in MHP shifts by approximately 400-500 meV to lower binding energy after SnO_2 deposition, mostly in accordance with the I 3d and Pb 4f core level shifts. The Cs $3d_{5/2}$ core level spectra exhibit a similar shift to lower binding energies. Hence, all MHP related core levels (e.g., Pb 4f, I 3d, N 1s, Cs $3d_{5/2}$) shift to lower binding energies upon ALD-SnO_2 deposition, providing evidence for an upward band bending in the MHP films towards the interface with the metal oxide overlayer.

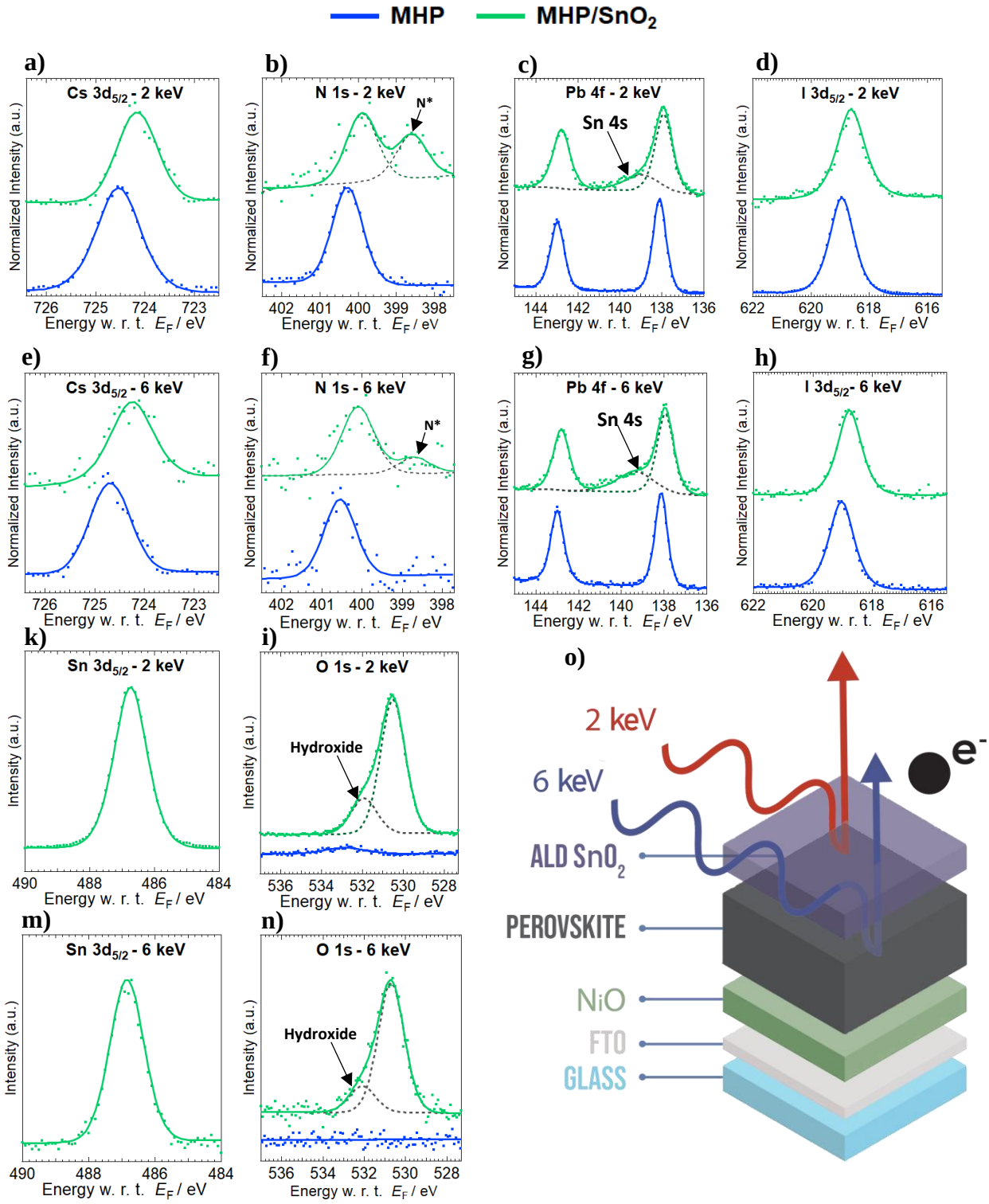

Figure 2: (a-n) HAXPES high-resolution spectra (including fit analysis of some core levels) of Cs $3d_{5/2}$, N 1s, Pb 4f, I $3d_{5/2}$, Sn $3d_{5/2}$, and O 1s of double cation MHP without (blue spectra) and with (green spectra) ALD SnO_2 top layers recorded using 2 and 6 keV excitation energy with Beryllium (Be) filter. N* indicates the peak component of a new nitrogen species as a reaction product of the ALD-SnO_2 deposition(o) Schematic of different probing depth of our HAXPES measurement using 2 keV and 6 keV photon energies.

We note that exposure to high-energy X-rays can induce damage to MHP samples, leading to inaccurate measurements of band bending.[36] To mitigate this issue, an aluminium (Al) filter was utilized to attenuate the 2 keV X-ray beam by a factor of 15 before it reached the sample in order to minimize the creation of defects that would shift the Fermi level and thereby impact the determination of band bending.

We analyzed the binding energy shift of the I $3d_{5/2}$ core level (measured on a fresh sample spot with the attenuated X-ray beam) as an indicator of the magnitude of band bending, which amounts to approximately 400 meV for both 2 keV and 6 keV photon energy (see Table S3, Figure S4 and further related discussion in S.I.). Assuming nearly flat band conditions at the MHP surface prior to interface formation as indicated by our HAXPES measurements of the bare MHP layer, this upward band bending corresponds to an interfacial electron extraction barrier which is detrimental to PSCs performance.

Next, we focus on the core levels of the SnO_2 film. The Sn $3d_{5/2}$ peak is located at 486.7 and 486.9 eV for 2 keV and 6 keV photon energy, respectively, corresponding to the Sn^{4+} state.[37] The shift in the binding energy of Sn $3d_{5/2}$ core level by 200 meV is similar to that observed for the Sn 4s levels discussed above and indicates a slight downward band bending in the SnO_2 film towards the MHP/SnO_2 interface, which would favor the transport of electrons towards the presumably defect-rich interface and thus again negatively affected PSC performance.

For the MHP/SnO_2 samples, we see the presence of two O 1s components using 2 keV and 6 keV photon energy. The O 1s peak located at 530.7 eV when using 6 keV corresponds to the SnO_2 contribution, while the same peak is shifted to a lower binding energy of 530.5 eV when using 2 keV, corroborating band bending in the SnO_2 film. The signals at 531.9 eV and 532.1 eV seen in the spectra acquired at 2 keV and 6 keV photon energy, respectively, are attributed to the presence of hydroxides.[21] These residual by-products, such as hydroxides, are commonly observed in low-temperature ALD processes and can typically be eliminated by post-annealing treatment at temperatures around 150-200°C.[38] However, in this case, the low thermal stability

of the MHP limits such post-heat treatment, as illustrated in Figure S1 (see S.I.). However, also the presence of "hydroxide" like species ascribed to surface adsorbates (particularly for the bare MHP sample) cannot be ruled out. This would be in line with the observation of one minor peak in the 2 keV data (blue line in Figure 2i), while this peak is below the noise floor of the HAXPES measurements in the 6 keV data (Figure 2n).

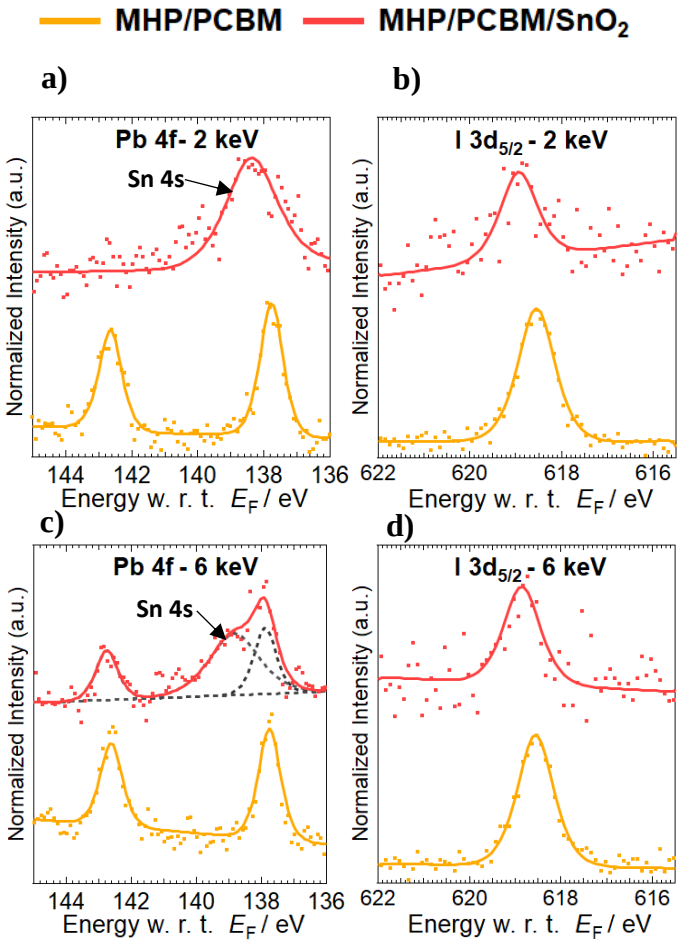

Figure3: HAXPES detail spectra of the Pb 4f and I 3d core levels for the samples with double cation MHP/PCBM hetero-interfaces with and without SnO_2 top layers measured using 2 and 6 keV excitations with Be filter. Curve fit results are included.

For comparison the HAXPES results of the samples with PCBM buffer layer deposited on MHP film with and without ALD-SnO_2 overlayer are shown in Figure 3. We use a 40 nm thick PCBM interlayer in this experiment to protect the MHP from the potentially detrimental effect of the interface formation with ALD-SnO_2. Detecting signal from the buried MHP layer, as shown in

Figure 3, beneath the PCBM layer of nominal thickness of 40 nm is unexpected for the 2 keV-excited measurements (the inelastic mean free path, or IMFP, of the photoelectrons in question is approximately 4 nm at 2 keV and 11 nm for 6 keV excitation, see S.I., Section 1.3) and hence suggests for the presence of pinholes in the PCBM layer, which is confirmed by corresponding scanning electron microscopy images (see S.I., Figure S2 (c)). We use this opportunity to compare the MHP core level data of these samples before and after ALD deposition. Because MHP-related signal for these samples can be collected only through the area of the pinholes of the PCBM films, i.e., sample regions with overlayers insufficiently thick to completely attenuate photoelectron signals originating from the buried MHP absorber, the obtained spectra of MHP core levels exhibit markedly low signal-to-noise ratios. As the Pb 4f and I 3d are the most prominent MHP-related lines, further data analysis is limited to spectra of these core levels. In addition, the absence of any discernible signal of the N 1s core level is of particular interest. This observation holds significant implications, as it suggests that the observed additional nitrogen contribution in the MHP/ALD-SnO_2 sample is not a mere by-product of the ALD process but instead arises from interfacial chemical reactions specific to the deposition directly on top of the MHP without buffer layer (see S.I., Figure S5).

After ALD SnO_2 deposition, the Pb 4f core-level spectra do not exhibit any signature of Pb at 2 keV photon energy, indicating that the MHP layer is buried under a closed PCBM and ALD SnO_2 layers, or that pinholes are sufficiently small/few that the Pb 4f signal, unlike the stronger I 3d, is not distinguishable from the background. Furthermore, this behavior indicates that iodine from the MHP might be migrating through the organic buffer layer towards the top interface. Here, as in Figure 3(a), we observe the Sn 4s peak at a binding energy of 138.2 eV. Whereas at 6 keV photon energy, we observe peaks corresponding to Pb 4f core-level spectra. After the ALD process, the I 3d core levels shift by almost 400 meV and 300 meV to higher binding energy, compared to the MHP/PCBM reference, for the 2 keV- and 6 keV-excited spectra, respectively. The peak shift observed can be linked to the creation of even small

amounts of donor states in the perovskite layer during the deposition process.[39] In comparison, the peaks corresponding to the Sn 3d and O 1s core levels for 2 keV and 6 keV photon energy still show a small shift which suggests that downward band bending in the SnO_2 film, as observed previously in the MHP/SnO_2 sample, is not fully mitigated (see S.I., Figure S5).

The present study demonstrates that the PCBM buffer layer inadequately protects the MHP layer from exposure to ALD precursors, as evidenced by the existence of pinholes. This inadequacy exerts a detrimental impact on the overall performance of the device, as indicated in Table S5. Therefore, we modified the recipe for deposition of the PCBM film to improve the coverage for PSCs fabrication as shown in Figure S3 (e). In the modified recipe, the PCBM solution in chlorobenzene is heated to 60°C prior to spin coating. The modified PCBM recipe is then incorporated to fabricate P-I-N PSCs (see S.I., Section 5). In this improved configuration, the PCBM interlayer eventually led to an improvement of the device characteristics with notably improved open circuit voltages above 1 V, which however require further optimization to obtain high fill factor values.

Moving forward, one of the key challenges that requires immediate attention is the effective mitigation of surface damage encountered by MHP materials during their initial exposure to ALD precursors. To address this issue, a promising avenue for exploration lies in the development of metalorganic and reaction precursors with reduced reactivity, aiming to minimize interfacial chemical reactions. Another intriguing possibility is the application of a suitable interlayer, such as two-dimensional (2D) perovskite or self-assembled molecules, between the MHP and ALD metal oxide films. The implementation of such interlayers presents a viable solution to shield the perovskite material from direct interaction with ALD precursors. These approaches hold significant potential in preserving the structural integrity and performance of MHPs and can ultimately contribute to the advancement and optimization of ALD processes for PSCs.

3. Conclusions

In summary, we report a synchrotron-based HAXPES interface investigation between MHP and ALD-SnO_2. This advanced characterization approach provided important information on the formation of new chemical species at the interface, i.e., a new nitrogen compound presumably from degraded formamidinium, as well as, lead dihalides. More in-depth analysis was performed to track the modification of band alignment induced by newly created interfacial defects. The Pb 4f, I 3d, N 1s, and Cs 3d core level peaks shifted to lower binding energy upon ALD-SnO_2 overlayer deposition; corresponding to an upward band bending inside the MHP at the interface, resulting in a significant electron barrier of over 400 meV and is therefore expected to negatively affect PCE performance of corresponding solar cells. Similarly, the observed downward band bending in the SnO_2 towards the interface is expected to limit PCE. The work is also extended to a system with a PCBM interlayer between MHP and SnO_2, which partly mitigates the chemical reaction when exposed to the ALD precursors. However, full protection against the degradation of the perovskite underneath is not achieved due to incomplete coverage of the PCBM layer on the MHP surface. In summary, this work acts as a guideline to explore alternative interlayers such as 2D perovskite or self-assembled organic molecules to chemically bind to the MHP species leading to a resilient protection against exposure to ALD precursors.

■ ASSOCIATED CONTENT

Supporting Information

Experimental Methods; Thermal stability of $FA_{0.7}Cs_{0.3}Pb(I_{0.9}Br_{0.1})_3$ MHP; Morphology of Perovskite, PCBM, and ALD SnO_2; HAXPES data and graphs; P-I-N Solar cell performances.

■ AUTHOR INFORMATION

Corresponding Author:

Philip Schulz - Institut Photovoltaïque d'Ile-de-France, UMR IPVF 9006, CNRS, École Polytechnique, Institut Polytechnique de Paris, 91120 Palaiseau, France;

Email : philip.schulz@cnrs.fr

Authors:

Nitin Mallik - Institut Photovoltaïque d'Ile-de-France, UMR IPVF 9006, CNRS, École Polytechnique, Institut Polytechnique de Paris, 91120 Palaiseau, France;

Javid Hajhemati - Institut Photovoltaïque d'Ile-de-France, UMR IPVF 9006, CNRS, École Polytechnique, Institut Polytechnique de Paris, 91120 Palaiseau, France;

Mathieu Fregnaux - Institut Lavoisier de Versailles, Université de Versailles Saint-Quentin-en-Yvelines, Université Paris-Saclay, CNRS, UMR 8180, 78035 Versailles Cedex, France;

Damien Coutancier - Institut Photovoltaïque d'Ile-de-France, UMR IPVF 9006, CNRS, 91120 Palaiseau, France;

Ashish Toby - Institut Photovoltaïque d'Ile-de-France, UMR IPVF 9006, CNRS, École Polytechnique, Institut Polytechnique de Paris, 91120 Palaiseau, France;

Shan-Ting Zhang - Institut Photovoltaïque d'Ile-de-France, 91120 Palaiseau, France;

Claudia Hartmann - Solar Energy Division, Helmholtz-Zentrum Berlin für Materialien und Energie GmbH (HZB), 12489, Berlin, Germany;

Elif Hüsam - Solar Energy Division, Helmholtz-Zentrum Berlin für Materialien und Energie GmbH (HZB), 12489, Berlin, Germany;

Ahmed Saleh - Solar Energy Division, Helmholtz-Zentrum Berlin für Materialien und Energie GmbH (HZB), 12489, Berlin, Germany;

Thomas Vincent - Institut Photovoltaïque d'Ile-de-France, 91120 Palaiseau, France;

Olivier Fournier – EDF**,** Institut Photovoltaïque d'Ile-de-France, 91120 Palaiseau, France;

Regan G. Wilks - Solar Energy Division, Helmholtz-Zentrum Berlin für Materialien und Energie GmbH (HZB, 12489, Berlin, Germany;

Damien Aureau - Institut Lavoisier de Versailles, Université de Versailles Saint-Quentin-en-Yvelines, Université Paris-Saclay, CNRS, UMR 8180, 78035 Versailles Cedex, France;

Roberto Félix - Solar Energy Division, Helmholtz-Zentrum Berlin für Materialien und Energie, 14109, Berlin, Germany;

Nathanaelle Schneider - Institut Photovoltaïque d'Ile-de-France, UMR IPVF 9006, CNRS, 91120 Palaiseau, France;

Marcus Bär - Solar Energy Division, Helmholtz-Zentrum Berlin für Materialien und Energie GmbH (HZB), 12489, Berlin, Germany; Dept. X-ray Spectroscopy at Interfaces of Thin Films, Helmholtz-Institute Erlangen-Nürnberg for Renewable Energy (HI ERN), 12489 Berlin, Germany ; Dept. of Chemistry and Pharmacy, Friedrich-Alexander-Universität Erlangen-Nürnberg (FAU), 91058 Erlangen, Germany ;

Author Contributions:

‖ N.M. and J.H. contributed equally to this work.

Notes: The authors declare no competing financial interest.

■ ACKNOWLEDGMENTS

This work was financially supported by the French Agence Nationale de la Recherche (ANR) with grant number: ANR-17-MPGA0012 and IPVF ANR-IEED-002-01. We thank Alexandre Blaizot for the SEM images. We thank HZB for the allocation of synchrotron radiation beamtime at BESSY II for HAXPES measurements.

■ REFERENCES

1. Min, H., Lee, D.Y., Kim, J., Kim, G., Lee, K.S., Kim, J., Paik, M.J., Kim, Y.K., Kim, K.S., Kim, M.G. and Shin, T.J., 2021. Perovskite solar cells with atomically coherent interlayers on SnO2 electrodes. *Nature*, *598*(7881), pp.444-450.
2. Jeon, N.J., Na, H., Jung, E.H., Yang, T.Y., Lee, Y.G., Kim, G., Shin, H.W., Il Seok, S., Lee, J. and Seo, J., 2018. A fluorene-terminated hole-transporting material for highly efficient and stable perovskite solar cells. *Nature Energy*, *3*(8), pp.682-689.
3. Schulz, P., 2018. Interface design for metal halide perovskite solar cells. *ACS Energy Letters*, *3*(6), pp.1287-1293.
4. Lira-Cantú, M., 2017. Perovskite solar cells: Stability lies at interfaces. *Nature Energy*, *2*(7), pp.1-3.
5. Christians, J.A., Schulz, P., Tinkham, J.S., Schloemer, T.H., Harvey, S.P., Tremolet de Villers, B.J., Sellinger, A., Berry, J.J. and Luther, J.M., 2018. Tailored interfaces of unencapsulated perovskite solar cells for> 1,000 hour operational stability. *Nature Energy*, *3*(1), pp.68-74.
6. Schulz, P., Cahen, D. and Kahn, A., 2019. Halide perovskites: is it all about the interfaces?. *Chemical reviews*, *119*(5), pp.3349-3417.
7. Wang, Q., Phung, N., Di Girolamo, D., Vivo, P. and Abate, A., 2019. Enhancement in lifespan of halide perovskite solar cells. *Energy & Environmental Science*, *12*(3), pp.865-886.

8. Shin, S.S., Lee, S.J. and Seok, S.I., 2019. Metal oxide charge transport layers for efficient and stable perovskite solar cells. *Advanced Functional Materials*, *29*(47), p.1900455.
9. Lee, Y., Lee, S., Seo, G., Paek, S., Cho, K.T., Huckaba, A.J., Calizzi, M., Choi, D.W., Park, J.S., Lee, D. and Lee, H.J., 2018. Efficient planar perovskite solar cells using passivated tin oxide as an electron transport layer. *Advanced Science*, *5*(6), p.1800130.
10. Jeong, S., Seo, S., Park, H. and Shin, H., 2019. Atomic layer deposition of a SnO_2 electron-transporting layer for planar perovskite solar cells with a power conversion efficiency of 18.3%. *Chemical communications*, *55*(17), pp.2433-2436.
11. Wang, H., Liu, H., Ye, F., Chen, Z., Ma, J., Liang, J., Zheng, X., Tao, C. and Fang, G., 2021. Hydrogen peroxide-modified SnO_2 as electron transport layer for perovskite solar cells with efficiency exceeding 22%. *Journal of Power Sources*, *481*, p.229160.
12. Ren, N., Zhu, C., Li, R., Mazumdar, S., Sun, C., Chen, B., Xu, Q., Wang, P., Shi, B., Huang, Q. and Xu, S., 2022. 50°C low-temperature ALD SnO_2 driven by H_2O_2 for efficient perovskite and perovskite/silicon tandem solar cells. *Applied Physics Letters*, *121*(3).
13. Raninga, R.D., Jagt, R.A., Béchu, S., Huq, T.N., Li, W., Nikolka, M., Lin, Y.H., Sun, M., Li, Z., Li, W. and Bouttemy, M., 2020. Strong performance enhancement in lead-halide perovskite solar cells through rapid, atmospheric deposition of n-type buffer layer oxides. *Nano Energy*, *75*, p.104946.
14. Ramos, F.J., Maindron, T., Béchu, S., Rebai, A., Frégnaux, M., Bouttemy, M., Rousset, J., Schulz, P. and Schneider, N., 2018. Versatile perovskite solar cell encapsulation by low-temperature ALD-Al_2O_3 with long-term stability improvement. *Sustainable Energy & Fuels*, *2*(11), pp.2468-2479.
15. Bush, K.A., Bailie, C.D., Chen, Y., Bowring, A.R., Wang, W., Ma, W., Leijtens, T., Moghadam, F. and McGehee, M.D., 2016. Thermal and environmental stability of semi-transparent perovskite solar cells for tandems enabled by a solution-processed nanoparticle buffer layer and sputtered ITO electrode. *Advanced Materials*, *28*(20), pp.3937-3943.
16. Wali, Q., Iftikhar, F.J., Khan, M.E., Ullah, A., Iqbal, Y. and Jose, R., 2020. Advances in stability of perovskite solar cells. *Organic Electronics*, *78*, p.105590.
17. Xing, Z., Xiao, J., Hu, T., Meng, X., Li, D., Hu, X. and Chen, Y., 2020. Atomic Layer Deposition of Metal Oxides in Perovskite Solar Cells: Present and Future. *Small Methods*, *4*(12), p.2000588.

18. Zardetto, V., Williams, B.L., Perrotta, A., Di Giacomo, F., Verheijen, M.A., Andriessen, R., Kessels, W.M.M. and Creatore, M., 2017. Atomic layer deposition for perovskite solar cells: research status, opportunities and challenges. *Sustainable Energy & Fuels*, *1*(1), pp.30-55.
19. Palmstrom, A.F., Raiford, J.A., Prasanna, R., Bush, K.A., Sponseller, M., Cheacharoen, R., Minichetti, M.C., Bergsman, D.S., Leijtens, T., Wang, H.P. and Bulović, V., 2018. Interfacial effects of tin oxide atomic layer deposition in metal halide perovskite photovoltaics. *Advanced Energy Materials*, *8*(23), p.1800591.
20. Dong, X., Hu, H., Lin, B., Ding, J. and Yuan, N., 2014. The effect of ALD-Zno layers on the formation of $CH_3NH_3PbI_3$ with different perovskite precursors and sintering temperatures. *Chemical communications*, *50*(92), pp.14405-14408.
21. Bracesco, A.E., Burgess, C.H., Todinova, A., Zardetto, V., Koushik, D., Kessels, W.M.E., Dogan, I., Weijtens, C.H., Veenstra, S., Andriessen, R. and Creatore, M., 2020. The chemistry and energetics of the interface between metal halide perovskite and atomic layer deposited metal oxides. *Journal of Vacuum Science & Technology A*, *38*(6).
22. Yang, Y., Zhang, Y., Bai, L., Malouangou, D.M., Matondo, J.T., Pan, J., Dai, S., Cai, M., Liu, X. and Guli, M., 2022. Research progress of atomic layer deposition technology to improve the long-term stability of perovskite solar cells. *Journal of Materials Chemistry C*, *10*(3), pp.819-839.
23. Park, H.H., 2021. Inorganic materials by atomic layer deposition for perovskite solar cells. *Nanomaterials*, *11*(1), p.88.
24. Raiford, J.A., Oyakhire, S.T. and Bent, S.F., 2020. Applications of atomic layer deposition and chemical vapor deposition for perovskite solar cells. *Energy & Environmental Science*, *13*(7), pp.1997-2023.
25. Brinkmann, K.O., Gahlmann, T. and Riedl, T., 2020. Atomic layer deposition of functional layers in planar perovskite solar cells. *Solar RRL*, *4*(1), p.1900332.
26. Seo, S., Jeong, S., Park, H., Shin, H. and Park, N.G., 2019. Atomic layer deposition for efficient and stable perovskite solar cells. *Chemical Communications*, *55*(17), pp.2403-2416.
27. Deng, K. and Li, L., 2016. Advances in the application of atomic layer deposition for organometal halide perovskite solar cells. *Advanced Materials Interfaces*, *3*(21), p.1600505.

28. Raiford, J.A., Chosy, C., Reeves, B.A. and Bent, S.F., 2021. Tailoring the Surface of Metal Halide Perovskites to Enable the Atomic Layer Deposition of Metal Oxide Contacts. *ACS Applied Energy Materials*, *4*(9), pp.9871-9880.

29. Hultqvist, A., Jacobsson, T.J., Svanström, S., Edoff, M., Cappel, U.B., Rensmo, H., Johansson, E.M., Boschloo, G. and Törndahl, T., 2021. SnO_X Atomic Layer Deposition on Bare Perovskite—An Investigation of Initial Growth Dynamics, Interface Chemistry, and Solar Cell Performance. *ACS applied energy materials*, *4*(1), pp.510-522.

30. Boyd, C.C., Cheacharoen, R., Leijtens, T. and McGehee, M.D., 2018. Understanding degradation mechanisms and improving stability of perovskite photovoltaics. *Chemical reviews*, *119*(5), pp.3418-3451.

31. Jain, S.M., Philippe, B., Johansson, E.M., Park, B.W., Rensmo, H., Edvinsson, T. and Boschloo, G., 2016. Vapor phase conversion of PbI_2 to $CH_3NH_3PbI_3$: Spectroscopic evidence for formation of an intermediate phase. *Journal of Materials Chemistry A*, *4*(7), pp.2630-2642.

32. Wu, W.Q., Rudd, P.N., Ni, Z., Van Brackle, C.H., Wei, H., Wang, Q., Ecker, B.R., Gao, Y. and Huang, J., 2020. Reducing surface halide deficiency for efficient and stable iodide-based perovskite solar cells. *Journal of the American Chemical Society*, *142*(8), pp.3989-3996.

33. Thampy, S., Zhang, B., Park, J.G., Hong, K.H. and Hsu, J.W., 2020. Bulk and interfacial decomposition of formamidinium iodide ($HC(NH_2)_2I$) in contact with metal oxide. *Materials Advances*, *1*(9), pp.3349-3357.

34. Gunasekar, G.H., Park, K., Ganesan, V., Lee, K., Kim, N.K., Jung, K.D. and Yoon, S., 2017. A covalent triazine framework, functionalized with Ir/N-heterocyclic carbene sites, for the efficient hydrogenation of CO_2 to formate. *Chemistry of Materials*, *29*(16), pp.6740-6748.

35. Bracesco, A.E., Jansen, J.W.P., Xue, H., Zardetto, V., Brocks, G., Kessels, W.M., Tao, S. and Creatore, M., 2023. In Situ IR Spectroscopy Studies of Atomic Layer-Deposited SnO2 on Formamidinium-Based Lead Halide Perovskite. *ACS Applied Materials & Interfaces*.

36. Milotti, V., Cacovich, S., Ceratti, D.R., Ory, D., Barichello, J., Matteocci, F., Di Carlo, A., Sheverdyaeva, P.M., Schulz, P. and Moras, P., 2023. Degradation and Self-Healing of FAPbBr3 Perovskite under Soft-X-Ray Irradiation. *Small Methods*, p.2300222.

37. Moulder, J.F., 1992. Handbook of X-ray Photoelectron Spectroscopy: A Reference Book of Standard Spectra for Identification and Interpretation of XPS Data, Physical Electronics Division, *Perkin-Elmer Corporation*, 978-0-9627026-2-4.

38. Elam, J.W., Baker, D.A., Hryn, A.J., Martinson, A.B., Pellin, M.J. and Hupp, J.T., 2008. Atomic layer deposition of tin oxide films using tetrakis (dimethylamino) tin. *Journal of Vacuum Science & Technology A*, *26*(2), pp.244-252.

39. Dunfield, S.P., Bojar, A., Cacovich, S., Frégnaux, M., Klein, T., Bramante, R., Zhang, F., Regaldo, D., Dufoulon, V., Puel, J.B. and Teeter, G., 2021. Carrier gradients and the role of charge selective contacts in lateral heterojunction all back contact perovskite solar cells. *Cell Reports Physical Science*, *2*(8).